Thin Solid Films 519 (2011) 5679–5683

Contents lists available at ScienceDirect

Thin Solid Films

journal homepage: www.elsevier.com/locate/tsf

# Structural and electronic properties of β-$In_2X_3$ (X = O, S, Se, Te) using *ab initio* calculations

S. Marsillac [a], N.S. Mangale [b], V. Gade [b], S.V. Khare [a,*]

[a] Department of Physics and Astronomy, The University of Toledo, Toledo, OH 43606, United States
[b] Department of Electrical Engineering and Computer Science, The University of Toledo, Toledo, OH 43606, United States

ARTICLE INFO

*Article history:*
Received 26 June 2010
Received in revised form 17 February 2011
Accepted 24 February 2011
Available online 11 March 2011

*Keywords:*
*Ab initio* calculations
Band structure
Cadmium sulphide
Electron density of states of crystalline solids
Local density approximation
Structure of specific crystalline solids

ABSTRACT

Several III-VI body-centered tetragonal layered compounds belonging to space group $I4_1/amd$ have been a subject of interest recently because of their potential applications in high efficiency and environmentally friendly copper–indium–gallium–selenide solar cells and molecules. Here we have studied the structural, energetic, and electronic properties of four compounds β-$In_2X_3$ (X = O, S, Se, Te), in this space group. Using first principles computations, we have fully determined the lattice constants *a* and *c*, as well as 10 internal parameters that define this unique structure of primitive unit cells of 40 atoms. For β-$In_2S_3$ our computed values are found to be consistent with experimental measurements. The bulk modulus B, local electronic density of states, total density of states, and band gap $E_g$ of these phases have been investigated.


## Introduction

Cu–In–Ga–S (CIGS) based solar cells are often considered as effective solar cell technologies for low-cost driven power generation. This is due to the fact that low material consumption for thin films and high deposition rate results in lower cost of large scale production. The major reason for the low cost is attributed to the high efficiency obtained at both cell and module level. A record efficiency of 18.8% was achieved with 0.5 $cm^2$ cell area by NREL [1]. CdS is one of the important layers in fabricating CIGS solar cells but poses ecological problems due to the presence of Cd; moreover it is deposited by a chemical bath which might be a problem in high deposition rate industrial processes [2]. Hence it is highly desirable to replace CdS by another material with similar or better properties. Compounds in the β-$In_2S_3$ family can be used as a substitute of CdS in high performing solar cells [2–4] but lack fundamental studies on their basic properties [5–11]. This material (β-$In_2S_3$) also has use in flat panel screen technology and other potential applications in photo-electronic devices. Group VI elements X (X = O, S, Se, or Te) form alloys with In which possess broad range of electronic and optical properties. Their theoretical study has been impeded by their large unit cell size of 40 atoms and a complex structure with 10 internal parameters with this cell.

## 2. Structural description

The four beta phases we have studied are body-centered tetragonal cell with a Pearson symbol tI80. They belong to the space group $I4_1/amd$ [12]. These structures are of the spinel-type with 4 ordered vacant tetrahedrally coordinated cation sites (Fig. 1) [13]. The unit cell consists of three spinel cubes stacked along the *c*-axis. All the octahedral sites in this spinel structure are occupied by an indium atom whereas out of 12 tetrahedral sites only 8 are occupied by an indium atom, i.e. 4 are vacant [14]. In each tetragonal unit cell of 40 atoms, there are 16 'In' layers and 24 'X' layers where X = O, S, Se, or Te. Table 1 gives a precise description of the specific positions of each atom in the unit cell corresponding to this type of stacking. There are ten internal degrees of freedom within this cell that describe the positions of these atoms. We denote these by $Y_M$ and $Z_M$, (M = 1, 2, 3, 4, 5) as shown in Table 1 [15]. Among the system β-$In_2X_3$, β-$In_2S_3$ has been the most widely studied semiconductor compound.

## 3. Computational method

We have performed *ab initio* total energy calculations within the local density approximation (LDA) to density functional theory [16] using the suit of codes VASP [17–20]. Core electrons are implicitly treated by ultra soft Vanderbilt type pseudopotentials [21] as supplied by G. Kresse and J. Hafner [22]. For each calculation, irreducible k-points are generated according to the Monkhorst-Pack scheme [23]. Convergence in energy differences is achieved with 5 k-points in the irreducible part of Brillouin zone for the forty atom unit cell described

* Corresponding author. Tel.: +1 419 530 2292; fax: +1 419 530 2723.
*E-mail address:* khare@physics.utoledo.edu (S.V. Khare).

0040-6090/$ – see front matter © 2011 Elsevier B.V. All rights reserved.
doi:10.1016/j.tsf.2011.02.092

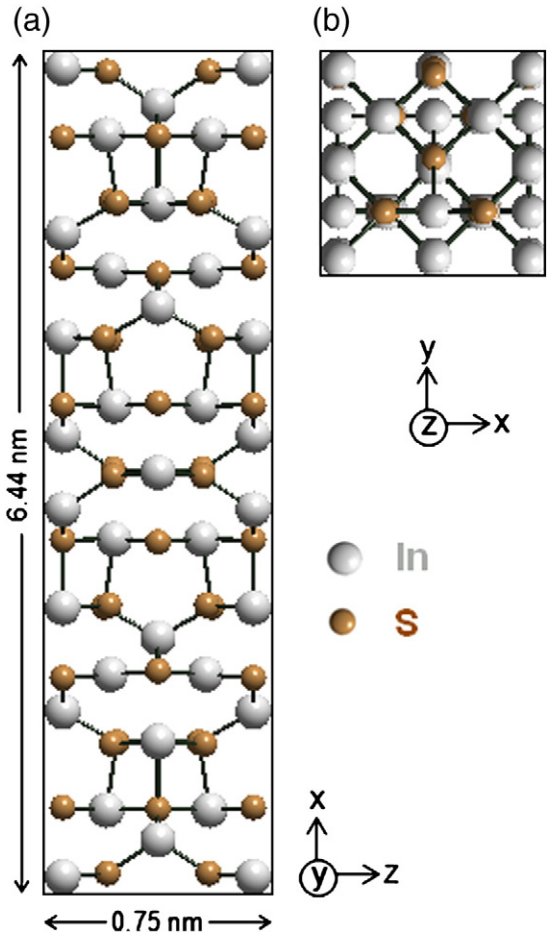


**Fig. 1.** Structure of β-$In_2S_3$ as viewed from (a) y-axis and (b) z-axis. The cell is a body centered tetragonal cell of spinel-type with 4 ordered vacant tetrahedrally coordinated cation sites. Cell size shown is twice that given in Table 1.

in Table 1. The single-particle wave functions have been expanded in a plane-wave basis using a 270 eV, 198 eV, 155 eV, and 115 eV kinetic energy cutoff for β-$In_2X_3$ (X = O, S, Se, Te) respectively. These values were determined to be sufficient by performing convergence tests. All atoms were allowed to relax until a force tolerance of 1 meV/Å was reached for each atom. The calculations for the total density of states (DOS) were performed with the tetrahedron method with Blöchl corrections for the energy [24].

To obtain the absolute minimum in total energy for each crystal structure, the equilibrium lattice constants $a$ and $c$ were varied independently. Once the equilibrium constants and corresponding volume $V_0 = a^2c/2$ were established for each structure, external strains $\delta$ of ±1%, and ±2% were applied to the structure, along all three lattice vectors while allowing full relaxation of the ions. This ionic relaxation allowed the internal parameters to change with the strain. We thus obtained the total minimum energies E (V) at these strained volumes V, corresponding to each value of $\delta$. These energies and strains were fit with the corresponding parabolic equation [25] $\Delta E = \frac{9}{2}V_0B\delta^2$, where $\Delta E \equiv E(V) - E(V_0)$. These fits yielded the value of the bulk modulus B.

## 4. Results and discussions

Our calculated values for the constants $a$, $c$, $c/a$, $V_0$, and B is shown in Table 2. The 10 internal structural parameters for each of these complex structures, which were determined in the process of finding the equilibrium lattice constant, are shown in Table 3. Experimental values of neutron powder method from Rampersadh et al. [13] for lattice constants, which are available only for β-$In_2S_3$, match our computed lattice structural parameters within an error of 2%. Our internal parameters for β-$In_2S_3$ also match with experiment closely, as seen from Table 3. Going down group VI from O to Te values of $a$, $c$, and $V_0$ increases while B, and the ratio $c/a$ decreases. The increase in the size of the anions as we go down the group may explain the increase in the lattice constants and the equilibrium volume.

As seen from Table 2, the bulk moduli (B) of β-$In_2X_3$ (X = O, S, Se, Te) were found to be 120.60, 62.14, 46.72, and 32.87 GPa respectively. It can be seen that the bulk modulus of β-$In_2X_3$ decreases significantly from β-$In_2O_3$ to β-$In_2S_3$ (≈45% decrease in B). This is related to the

**Table 1**
The table lists forty atom bases for the unit cell of $In_2S_3$ [15]. The lattice vectors of this body centered tetragonal structure with lattice constants $a$ and $c$ are given in Cartesian coordinates as: $a_1 = a\,(1, 0, 0)$, $a_2 = a\,(0, 1, 0)$, and $a_3 = a\,(½, ½, r/2)$, where $r = c/a$, and the basis vectors are shown below. The constant "$Z_M$" and "$Y_M$" (where M = 1, 2, 3, 4, 5) corresponding to internal degrees of freedom. Computed values for the lattice constants and internal degrees of freedom are given in Tables 2 and 3.

| Atom Type | Basis atom number | Position Vector |
|---|---|---|
| In | $B_1$ | 0 |
| In | $B_2$ | ½ $\mathbf{a}_2$ |
| In | $B_3$ | −½ $\mathbf{a}_2$ + ½ $\mathbf{a}_3$ |
| In | $B_4$ | −½ $\mathbf{a}_1$ − ½ $\mathbf{a}_2$ + ½ $\mathbf{a}_3$ |
| In | $B_5$ | $-Z_1\,\mathbf{a}_1 + (Y_1 - Z_1)\,\mathbf{a}_2 + 2\,Z_1\,\mathbf{a}_3$ |
| In | $B_6$ | $-Z_1\,\mathbf{a}_1 + (½ - Y_1 - Z_1)\,\mathbf{a}_2 + 2\,Z_1\,\mathbf{a}_3$ |
| In | $B_7$ | $-(Y_1 + Z_1)\,\mathbf{a}_1 + (½ - Z_1)\,\mathbf{a}_2 + (½ + 2\,Z_1)\,\mathbf{a}_3$ |
| In | $B_8$ | $-(½ - Y_1 + Z_1)\,\mathbf{a}_1 - (½ + Z_1)\,\mathbf{a}_2 + (½ + 2\,Z_1)\,\mathbf{a}_3$ |
| In | $B_9$ | $Z_1\,\mathbf{a}_1 + (½ + Y_1 + Z_1)\,\mathbf{a}_2 - 2\,Z_1\,\mathbf{a}_3$ |
| In | $B_{10}$ | $Z_1\,\mathbf{a}_1 - (Y_1 - Z_1)\,\mathbf{a}_2 - 2\,Z_1\,\mathbf{a}_3$ |
| In | $B_{11}$ | $(Y_1 + Z_1)\,\mathbf{a}_1 + (½ + Z_1)\,\mathbf{a}_2 + (½ - 2\,Z_1)\,\mathbf{a}_3$ |
| In | $B_{12}$ | $-(½ + Y_1 - Z_1)\,\mathbf{a}_1 - (½ - Z_1)\,\mathbf{a}_2 + (½ - 2\,Z_1)\,\mathbf{a}_3$ |
| In | $B_{13}$ | $-Z_2\,\mathbf{a}_1 + (¼ - Z_2)\,\mathbf{a}_2 + 2\,Z_2\,\mathbf{a}_3$ |
| In | $B_{14}$ | $-(¼ + Z_2)\,\mathbf{a}_1 + (½ - Z_2)\,\mathbf{a}_2 + (½ + 2\,Z_2)\,\mathbf{a}_3$ |
| In | $B_{15}$ | $Z_2\,\mathbf{a}_1 - (¼ - Z_2)\,\mathbf{a}_2 - 2\,Z_2\,\mathbf{a}_3$ |
| In | $B_{16}$ | $(¼ + Z_2)\,\mathbf{a}_1 + (½ + Z_2)\,\mathbf{a}_2 + (½ - 2\,Z_2)\,\mathbf{a}_3$ |
| S | $B_{17}$ | $-Z_3\,\mathbf{a}_1 + (Y_3 - Z_3)\,\mathbf{a}_2 + 2\,Z_3\,\mathbf{a}_3$ |
| S | $B_{18}$ | $-Z_3\,\mathbf{a}_1 + (½ - Y_3 - Z_3)\,\mathbf{a}_2 + 2\,Z_3\,\mathbf{a}_3$ |
| S | $B_{19}$ | $-(Y_3 + Z_3)\,\mathbf{a}_1 + (½ - Z_3)\,\mathbf{a}_2 + (½ + 2\,Z_3)\,\mathbf{a}_3$ |
| S | $B_{20}$ | $-(½ - Y_3 + Z_3)\,\mathbf{a}_1 - (½ + Z_3)\,\mathbf{a}_2 + (½ + 2\,Z_3)\,\mathbf{a}_3$ |
| S | $B_{21}$ | $Z_3\,\mathbf{a}_1 + (½ + Y_3 + Z_3)\,\mathbf{a}_2 - 2\,Z_3\,\mathbf{a}_3$ |
| S | $B_{22}$ | $Z_3\,\mathbf{a}_1 - (Y_3 - Z_3)\,\mathbf{a}_2 - 2\,Z_3\,\mathbf{a}_3$ |
| S | $B_{23}$ | $(Y_3 + Z_3)\,\mathbf{a}_1 + (½ + Z_3)\,\mathbf{a}_2 + (½ - 2\,Z_3)\,\mathbf{a}_3$ |
| S | $B_{24}$ | $-(½ + Y_3 - Z_3)\,\mathbf{a}_1 - (½ - Z_3)\,\mathbf{a}_2 + (½ - 2\,Z_3)\,\mathbf{a}_3$ |
| S | $B_{25}$ | $-Z_4\,\mathbf{a}_1 + (Y_4 - Z_4)\,\mathbf{a}_2 + 2\,Z_4\,\mathbf{a}_3$ |
| S | $B_{26}$ | $-Z_4\,\mathbf{a}_1 + (½ - Y_4 - Z_4)\,\mathbf{a}_2 + 2\,Z_4\,\mathbf{a}_3$ |
| S | $B_{27}$ | $-(Y_4 + Z_4)\,\mathbf{a}_1 + (½ - Z_4)\,\mathbf{a}_2 + (½ + 2\,Z_4)\,\mathbf{a}_3$ |
| S | $B_{28}$ | $-(½ - Y_4 + Z_4)\,\mathbf{a}_1 - (½ + Z_4)\,\mathbf{a}_2 + (½ + 2\,Z_4)\,\mathbf{a}_3$ |
| S | $B_{29}$ | $Z_4\,\mathbf{a}_1 + (½ + Y_4 + Z_4)\,\mathbf{a}_2 - 2\,Z_4\,\mathbf{a}_3$ |
| S | $B_{30}$ | $Z_4\,\mathbf{a}_1 - (Y_4 - Z_4)\,\mathbf{a}_2 - 2\,Z_4\,\mathbf{a}_3$ |
| S | $B_{31}$ | $(Y_4 + Z_4)\,\mathbf{a}_1 + (½ + Z_4)\,\mathbf{a}_2 + (½ - 2\,Z_4)\,\mathbf{a}_3$ |
| S | $B_{32}$ | $-(½ + Y_4 - Z_4)\,\mathbf{a}_1 - (½ - Z_4)\,\mathbf{a}_2 + (½ - 2\,Z_4)\,\mathbf{a}_3$ |
| S | $B_{33}$ | $-Z_5\,\mathbf{a}_1 + (Y_5 - Z_5)\,\mathbf{a}_2 + 2\,Z_5\,\mathbf{a}_3$ |
| S | $B_{34}$ | $-Z_5\,\mathbf{a}_1 + (½ - Y_5 - Z_5)\,\mathbf{a}_2 + 2\,Z_5\,\mathbf{a}_3$ |
| S | $B_{35}$ | $-(Y_5 + Z_5)\,\mathbf{a}_1 + (½ - Z_5)\,\mathbf{a}_2 + (½ + 2\,Z_5)\,\mathbf{a}_3$ |
| S | $B_{36}$ | $-(½ - Y_5 + Z_5)\,\mathbf{a}_1 - (½ + Z_5)\,\mathbf{a}_2 + (½ + 2\,Z_5)\,\mathbf{a}_3$ |
| S | $B_{37}$ | $Z_5\,\mathbf{a}_1 + (½ + Y_5 + Z_5)\,\mathbf{a}_2 - 2\,Z_5\,\mathbf{a}_3$ |
| S | $B_{38}$ | $Z_5\,\mathbf{a}_1 - (Y_5 - Z_5)\,\mathbf{a}_2 - 2\,Z_5\,\mathbf{a}_3$ |
| S | $B_{39}$ | $(Y_5 + Z_5)\,\mathbf{a}_1 + (½ + Z_5)\,\mathbf{a}_2 + (½ - 2\,Z_5)\,\mathbf{a}_3$ |
| S | $B_{40}$ | $-(½ + Y_5 - Z_5)\,\mathbf{a}_1 - (½ - Z_5)\,\mathbf{a}_2 + (½ - 2\,Z_5)\,\mathbf{a}_3$ |

**Table 2**
Equilibrium properties of the tetragonal unit cell in Table 1: the lattice constants $a$ and $c$, their ratio $c/a$, equilibrium volume $V_0$, bulk modulus B and electronic band gap $E_g$. Experimental values from Ref. [13].

| Property | β-$In_2O_3$ | β-$In_2S_3$ Theory | β-$In_2S_3$ Experiment | β-$In_2Se_3$ | β-$In_2Te_3$ |
|---|---|---|---|---|---|
| $a$ (Å) | 6.32 | 7.50 | 7.60 | 7.95 | 8.71 |
| $c$ (Å) | 27.20 | 32.20 | 32.35 | 33.16 | 34.28 |
| $c/a$ | 4.30 | 4.29 | 4.26 | 4.17 | 3.94 |
| $V_0 = a^2c/2$ (Å$^3$) | 543.26 | 906.50 | 937.93 | 1048.85 | 1300.31 |
| B (GPa) | 120.60 | 62.14 | | 46.72 | 32.87 |
| $E_g$ (eV) | 0.6 | 1.02 | | 0.23 | 0 |

**Table 3**
Computed values of the dimensionless parameters "$Y_M$" and "$Z_M$" (defined in Table 1) corresponding to internal degrees of freedom for β-$In_2O_3$, β-$In_2S_3$, β-$In_2Se_3$ and β-$In_2Te_3$. Experimental values are from Ref. [13].

| | β-$In_2O_3$ | β-$In_2S_3$ | | β-$In_2Se_3$ | β-$In_2Te_3$ |
|---|---|---|---|---|---|
| | | Theoretical | Experiment | | |
| $Y_1$ | −0.007515 | −0.021255 | −0.0201 | −0.023265 | −0.036737 |
| $Y_2$ | 0.250000 | 0.250000 | 0.2500 | 0.250000 | 0.250000 |
| $Y_3$ | −0.002573 | −0.005846 | −0.0160 | −0.010579 | −0.016192 |
| $Y_4$ | 0.029477 | 0.005619 | 0.0060 | 0.004753 | 0.000550 |
| $Y_5$ | 0.021686 | 0.021310 | 0.0333 | 0.026458 | 0.032940 |
| $Z_1$ | 0.332512 | 0.333534 | 0.3324 | 0.334529 | 0.337477 |
| $Z_2$ | 0.204951 | 0.203723 | 0.2044 | 0.204115 | 0.204874 |
| $Z_3$ | 0.250872 | 0.250754 | 0.2457 | 0.251101 | 0.250249 |
| $Z_4$ | 0.074560 | 0.078484 | 0.0859 | 0.080194 | 0.085095 |
| $Z_5$ | 0.412490 | 0.413665 | 0.4164 | 0.413740 | 0.416345 |

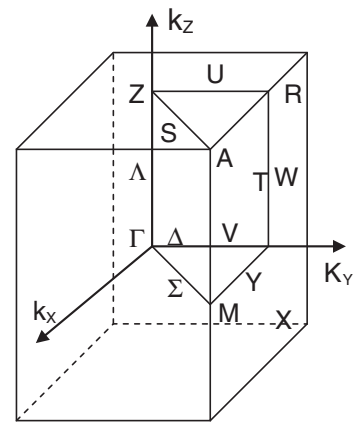


**Fig. 3.** Brillouin zone for tetragonal structure.

hardness of the oxides generally observed in many structural motifs. This has been reported in various other studies as well [26–28]. However, the decrease in B from β-$In_2S_3$ to β-$In_2Se_3$ to β-$In_2Te_3$ is very small.

We calculated the electronic band structure of these materials as shown in Fig. 2. The special k-points are marked on the shape of the first Brillouin zone, for the tetragonal structure, in Fig. 3 [29]. We observe from Fig. 2, that the band gaps $E_g$ are 0.6 eV, 1.02 eV, 0.23 eV and 0 eV for β-$In_2X_3$ (X = O, S, Se, Te) respectively. It was observed that β-$In_2O_3$ has a direct band gap, β-$In_2S_3$ and β-$In_2Se_3$ have indirect band gaps and β-$In_2Te_3$ was found with no band gap. It can be seen that for β-$In_2O_3$ the direct band gap occurs at Γ whereas for β-$In_2S_3$ and β-$In_2Se_3$ the indirect band gap is between Γ and X. We have observed a band gap of 1.09 eV for β-$In_2S_3$, which is 50% of the reported experimental value [30], as is expected from the LDA approximation that we have used. We note that LDA is well known to underestimate band gaps significantly and our $E_g$ values cannot directly be compared with experiment, for $In_2Se_3$ and $In_2Te_3$. The band gaps decrease as expected from S to Te [31]. However, the gap for β-$In_2O_3$ is surprisingly low. It is known that for oxides the LDA gap error can be very large [32] so we expect the true gap to be much larger in this case and hence larger than that for $In_2S_3$. We also observe that bands between M and A and between Z and Γ have low dispersion signifying tightly bound states along z-axis of the crystals, i.e. between layers. Along the other directions A–R–Z and Γ–X–M we observe very dispersive bands showing more distributed free electron like behavior within each layer.

The local density of states (LDOS) showing the hybridization of the various β-$In_2X_3$ (X = O, S, Se, Te) electronic states is shown in Fig. 4. LDOS shows interesting features: the hybridization peaks of X p (X = O, S, Se) and In p lie between −1 eV and −2 eV, while those of In p and Te p are between −3 eV and −4 eV. This suggests that the In p and Te p bonds are stronger than In p and X p (X = O, S, Se) bonds. The excited states show a tendency for increasing overlap between the In p and X p states as we go down the column for X (X = O, S, Se, Te). These states also show a tendency to approach $E_f$ and hence to keep reducing $E_g$ for values of X from S to Te.

Our calculated total density of states (DOS) is shown in Fig. 5. The highest peak in the DOS shifts towards the Fermi energy $E_f$ as we go down the cation group for β-$In_2X_3$ (X = O, S, Se, Te). This matches the

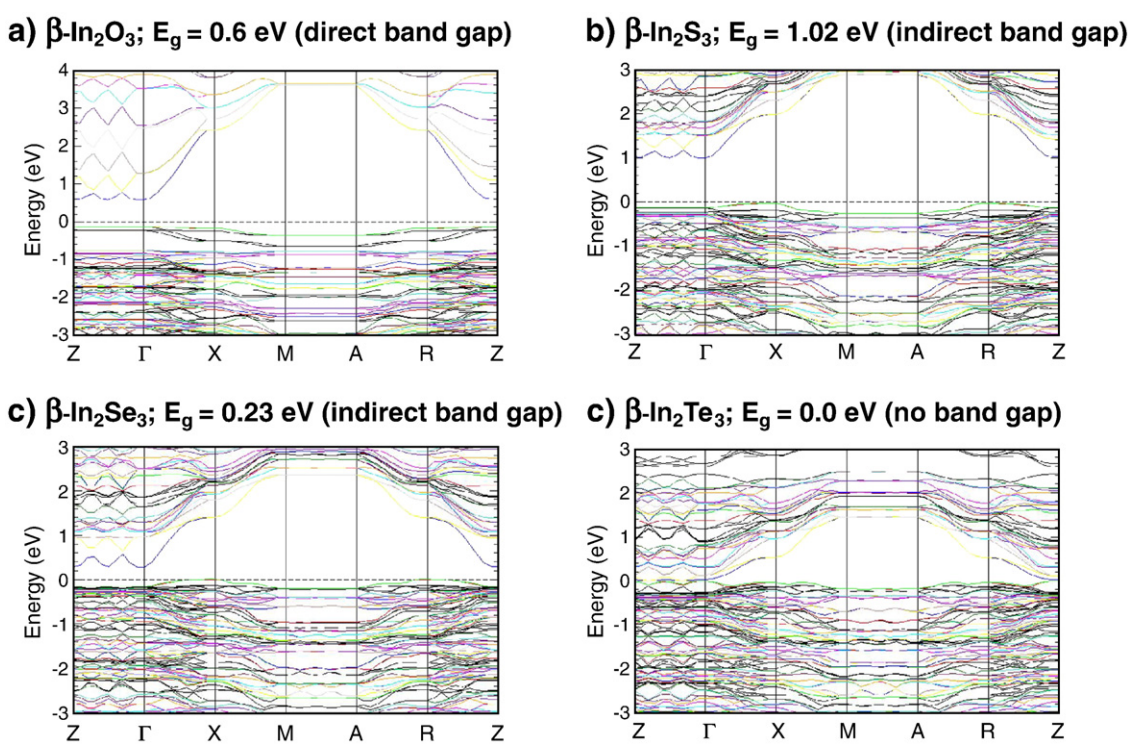


**Fig. 2.** Electronic band structures for β-$In_2X_3$ (X = O, S, Se, Te) are studied. The zero of the energy is taken at the Fermi energy $E_f$ shown by a dotted line.

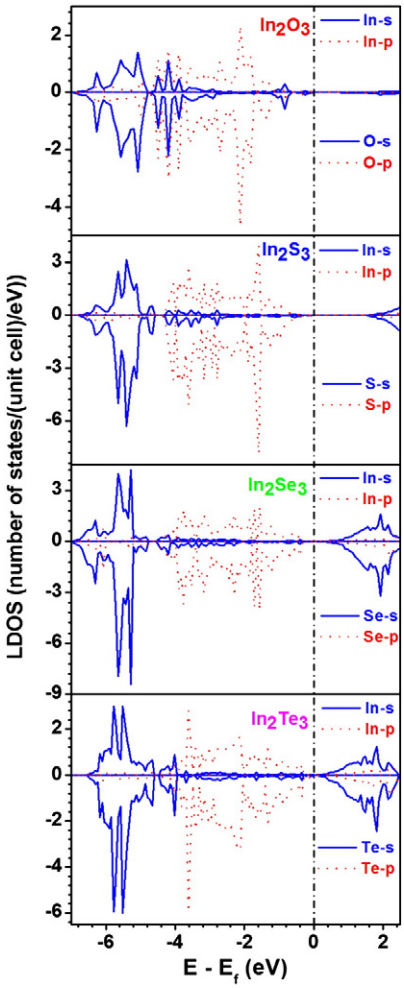


**Fig. 4.** Local density of states (LDOS) for β-$In_2X_3$ (X = O, S, Se, Te). The LDOS for the s states are not shown since they do not contribute much to bonding. The zero of the energy is taken at the Fermi energy $E_f$ shown by a dotted line.

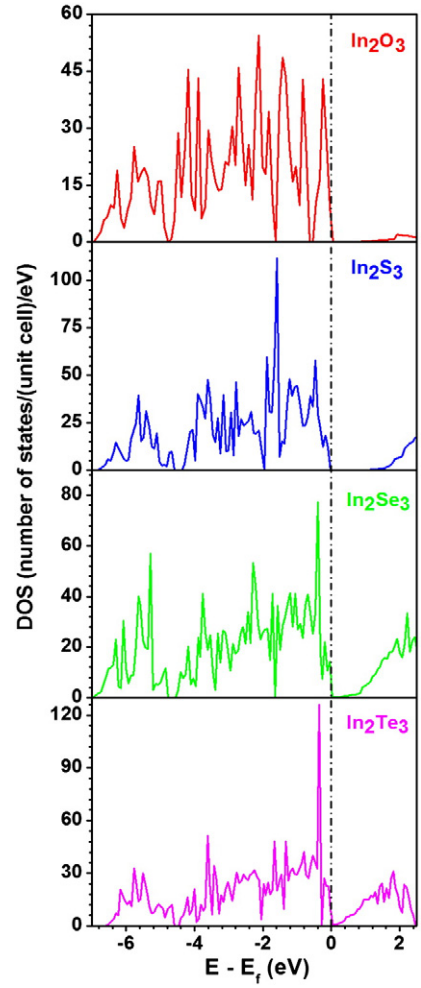


**Fig. 5.** The total density of states (DOS) is shown as a function of energy for β-$In_2X_3$ (X = O, S, Se, Te) studied. The zero of the energy is taken at the Fermi energy $E_f$ shown by a dotted line.

trend of the lowering of the band gaps in these systems. The maximum value of the DOS for β-$In_2O_3$ is much lower than in the other three cases. It could be related to errors in the LDA and generalized gradient approximation, as applied to oxygen compounds that have been observed earlier [32–35].

## 5. Conclusions

In summary we have characterized the structural and electronic properties of four compounds β-$In_2X_3$ (X = O, S, Se, Te) using *ab initio* computations. We fully determined the lattice constants *a* and *c*, as well as 10 internal parameters that define this unique structure of primitive unit cells of 40 atoms. The bulk modulus B, local electronic density of states (LDOS), total density of states (DOS), and band gap $E_g$ of these phases have been investigated. Going down group VI from O to Te values of *a*, *c*, and $V_0$ increase while B and the ratio *c*/*a* decrease. It was observed that β-$In_2O_3$ has a direct band gap, β-$In_2S_3$ and β-$In_2Se_3$ have indirect band gaps and β-$In_2Te_3$ has no band gap within the LDA. Due to well known errors in LDA we expect β-$In_2Te_3$ to be either metallic or a semi-conductor. The LDOS shows an increasing tendency of excited p states of In and X to overlap as we go from S to Te.

## Acknowledgments

We thank the Ohio Supercomputing Centre and National Centre for Supercomputing Applications for computing resources. We thank the Wright Center for Photovoltaic Innovation and Commercialization, National Science Foundation (#DMR0705464, #CNS0855134), DARPA for financial support.

## References

[1] A.M. Contreras, B. Egaas, K. Ramanathan, J. Hiltner, A. Swartzlander, F. Hasoon, R. Noufi, Prog. Photovolt. Res. Appl. 7 (1999) 311.
[2] S. Spiering, A. Eicke, D. Hariskos, M. Powalla, N. Naghavi, D. Lincot, J. Thin Solid Films 451 (452) (2004) 562.
[3] J.F. Trigo, B. Asenjo, J. Herrero, M.T. Gutierrez, Sol. Energy Sol. Cells 92 (2008) 1145.
[4] S. Gall, N. Barreau, F. Jacob, S. Harel, J. Kessler, Thin Solid Films 515 (2007) 6076.
[5] H. Xin Bai, L. Xing Zhang, Y. Cai Zhang, Mater. Lett. 63 (2009) 823.
[6] D. Andrea, K.R. Angel, Poeppelmeier, J. Solid State Chem. 153 (2000) 41.
[7] S.M. Rozati, T. Ganj, J. Appl. Sci. 2 (2005) 1106.
[8] R.A. Ismail, D.N. Raouf, D.F. Raouf, J. Opt. Adv. Mater. 8 (2006) 1443.
[9] H.T. El-Shair, A.E. Bekheet, J. Phys. D Appl. Phys. 25 (1992) 1122.
[10] J. Van Landuyt, G. Van Tendeloo, Phys. Status Solidi 30 (1975) 299.
[11] C. Julien, M. Eddrief, Thin Solid Films 137 (1986) 27.
[12] N.A. Hegab, M.A. Afifi, A.E. El-Shazly, A.E. Bekheet, J. Mater. Sci. 33 (1998) 2441.
[13] N.S. Rampersadh, A.M. Venter, D.G. Billing, Phys. B 350 (2004) E383.
[14] N. Barreau, J.C. Bernede, C. Deudon, L. Brohan, S. Marsillac, J. Cryst. Growth 241 (2002) 4.
[15] http://cst-www.nrl.navy.mil/lattice/struk/bIn2S3.html.
[16] P. Hohenberg, W. Kohn, Phys. Rev. 136 (1964) B864; W. Kohn, L.J. Sham, Phys. Rev. 140 (1965) A1133.
[17] G. Kresse, J. Hafner, Phys. Rev. B 47 (1993) 558.
[18] G. Kresse, Thesis, Technische Universiät Wien, Austria, 1993.
[19] G. Kresse, J. Furthmüller, Comput. Mater. Sci. 6 (1996) 15.
[20] G. Kresse, J. Furthmüller, Phys. Rev. B 54 (1996) 11169.
[21] D. Vanderbilt, Phys. Rev. B 41 (1990) 7892.
[22] G. Kresse, J. Hafner, J. Phys. Condens. Matter 6 (1994) 8245.

[23] H.J. Monkhorst, J.D. Pack, Phys. Rev. B 13 (1976) 5188.
[24] P.E. Blöchl, Phys. Rev. B 50 (1994) 17953.
[25] L. Fast, J.M. Wills, B. Johansson, O. Eriksson, Phys. Rev. B 51 (1995) 17431.
[26] N. Kaiser, H.K. Pulker, Optical Interference Coatings, Springer-Verlag, Berlin, 2003.
[27] P.J. Martin, A. Bendavid, M.V. Swain, R.P. Netterfield, T.J. Kinder, W.G. Sainty, D. Grace, Mater. Res. Soc. Symp. Proc. 308 (1993) 583.
[28] D.S. Liu, Y.K. Liao, C.Y. Wu, F.S. Juang, C.T. Lee, Mater. Sci. Forum 505–507 (2006) 439.
[29] B.I. Min, Y.-R. Jang, Phys. Rev. B 44 (1991) 13270.
[30] N. Revathi, P. Prathap, Y.P.V. Subbaiah, K.T. Ramakrishna Reddy, J. Phys. D Appl. Phys. 41 (2008) 1555404.
[31] M.V. Schilfgaarde, T. Kotani, S. Faleev, Phys. Rev. Lett. 96 (2006) 226402.
[32] L. Wang, T. Maxisch, G. Ceder, Phys. Rev. B 73 (2006) 195107.
[33] R.O. Jones, O. Gunnarsson, Rev. Mod. Phys. 61 (1989) 689.
[34] D.C. Patton, D.V. Porezag, M.R. Pederson, Phys. Rev. B 55 (1997) 7454.
[35] B. Hammer, L.B. Hansen, J.K. Nørskov, Phys. Rev. B 59 (1999) 7413.